Sensitivity Estimates and Backgrounds Studies for Phase-I and II of the COMET Experiment

Benjamin Edward Krikler
of Imperial College London

A dissertation submitted to Imperial College London
for the degree of Doctor of Philosophy

Abstract

Declaration

This dissertation is the result of my own work, except where explicit reference is made to the work of others, and has not been submitted for another qualification to this or any other university. This dissertation does not exceed the word limit for the respective Degree Committee.

Benjamin Edward Krikler

Acknowledgements

Contents

Chapter 1.

The COMET Experiment

The aim of the COMET experiment is to search for COherent Muon to Electron Transitions with a single-event-sensitivity of around 3×10^{-17}. This amounts to an improvement of four orders of magnitude compared to the current limit [1] which requires some significant changes to the way the experiment operates.

The general experimental goals of COMET are to:

- stop many muons in aluminium,
- have a high signal acceptance,
- suppress potential background sources to well below a single event.

At the level of sensitivity desired for COMET these requirements translate to the need for:

- a very high intensity muon beam,
- a thin stopping target and low material budget detector,
- a low energy muon beam,
- a pulse beam and relatively low-Z stopping target.

Realising these goals requires many new experimental techniques and as such COMET has decided to operate in two stages, Phase-I and Phase-II. Phase-II will realise the final objective of 3×10^{-17}, whilst Phase-I is only aiming for 3×10^{-15}. Although Phase-I will run sooner, since it is heavily motivated by Phase-II, I shall describe Phase-II in more depth first and return Phase-I subsequently. Firstly however I will discuss some of the key aspects common to both Phase-I and Phase-II.

1.1. Proton Beam Energy and Production Target

((CHECK: Figure for pion vs. antiproton production cross-section))

1.2. Particle Transport through Bent Solenoids

The dynamics of a charged particle in a magnetic field is determined by the Lorentz equation:

$$\vec{F} = \frac{q}{m}\vec{p} \times \vec{B} \tag{1.1}$$

where q, $\vec{p}$ and m are the particle's charge, momentum and mass respectively, and $\vec{B}$ is the magnetic field. In a uniform magnetic field where all field lines are parallel, clearly the motion of the particle follows a helix whose axis is parallel to the field and with a helical pitch-angle given by:

$$\theta = \tan^{-1}\left(\frac{P_{\mathrm{T}}}{P_{\mathrm{L}}}\right) \tag{1.2}$$

where P_{T} and P_{L} are respectively the transverse and longitudinal components of the momentum with respect to the magnetic field. Such a field can be realised to a high precision by a cylindrical solenoid coil.

If instead one were to bend a solenoid coil, so that it's axis describes a circular arc, two effects are introduced: firstly, the uniformity of the field is changed such that a higher magnetic field is found on the inside of the bend, and secondly the field lines also bend. Each of these changes causes the motion of the particle to deviate from that of a straight solenoid. Whilst one can think of the particle as following a helix around the field lines still, the centre of this helix can be shown to drift out of the plane of the bending. Firstly, the radial gradient introduced to the field causes a drift which is proportional to the transverse momentum of the particle. Secondly, the centrifugal pseudo-force as the particle tracks the now cylindrical field lines, creates a force that acts perpendicularly to the magnetic field. Since the field lines follow the solenoidal axis, this also produces a vertical drift, proportional to the longitudinal momentum, however.

Taken together, the result is a vertical drift with a velocity given by:

(1.3)

1.3. Stopping Target Material and Beam Pulsing

1.4. COMET Phase-II

COMET Phase-II will be the final stage of the experiment. It will make use of all the above techniques

1.5. COMET Phase-I

1.6. Status and Schedule

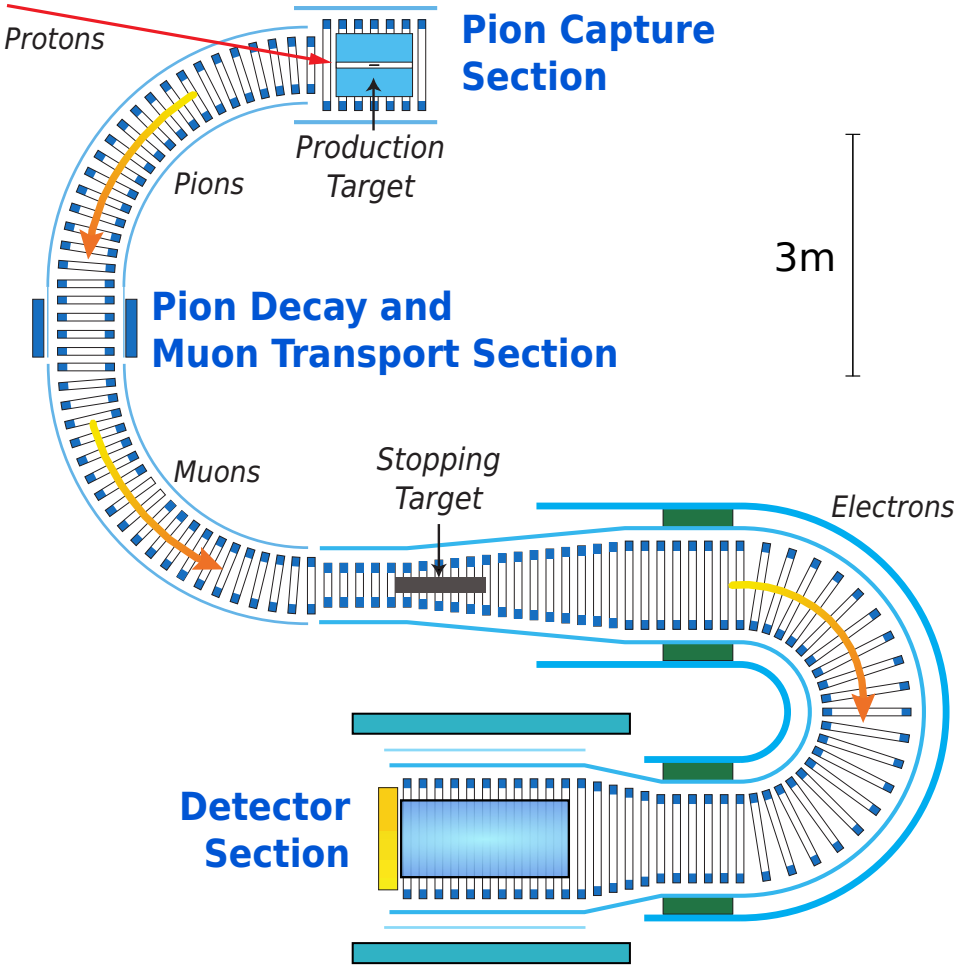

Figure 1.1.: Schematic layout of COMET Phase-II. The 8 GeV proton beam enters from the top-left, producing (amongst other things) pions. Pions and muons travelling backwards with respect to the proton beam are then transported around 180 degrees of bent solenoid, during which time most of the pions decay producing an intense muon beam. About 40% of these muons then stop in the stopping target (centre of image). Any electrons coming from μ-e conversion are then transported through another 180 degrees of bent solenoid into the detector system.

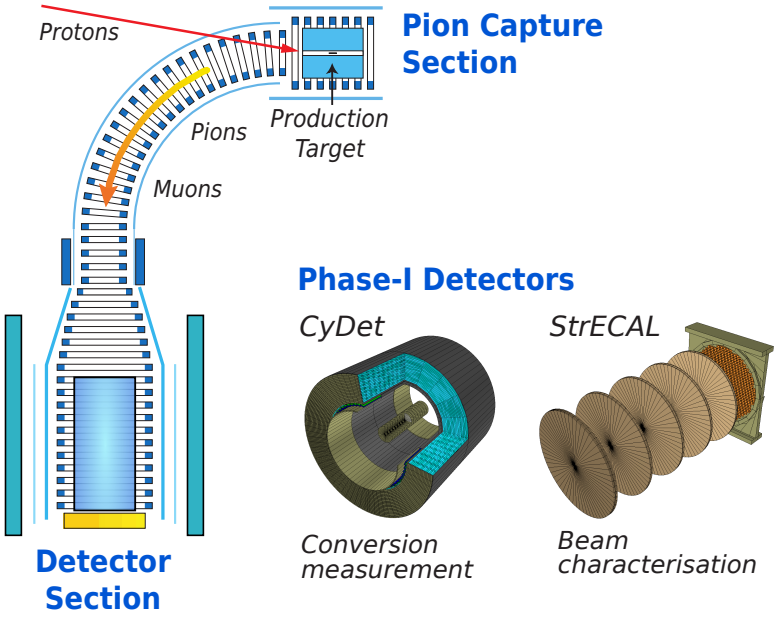

Figure 1.2.: Schematic layout of COMET Phase-I.

Chapter 2.

Phase-II Optimisation

1. Before a substantial sensitivity estimate can be made, need a solidly optimised design

2. Aiming for 3×10^{-17} within a single year of running

3. Designs previously optimised [**?**], and these results are used as nominal design / starting point

4. Fresh optimisation using new software / simulation, updated fieldmaps, physics lists and geometry

5. Some aspects fixed already since Phase-I under construction: Experiment hall, Torus1, detector solenoid, fieldmap and coil parameters?

6. Key areas for optimising:

6.1. Production target dimensions

6.2. Torus1 dipole field strength

6.3. Torus2 dipole field strength

6.4. Electron spectrometer dipole field strength

6.5. collimator shapes and locations

6.6. stopping target and beam blocker position and form

6.7. DIO blockers on spectrometer

2.1. Optimisation Strategy

7. Take some aspects as fixed

8. Limit scope and approach:

8.1. Ideally, each aspect optimised in combination to maximise signal acceptance and reduce background

8.2. How decoupled are each section?

8.3. In practise such an optimisation is not easy to do, instead aim to produce a baseline optimisation so that all backgrounds / issues can be identified

8.4. This can then form basis for further optimisation, with perhaps a smarter more integrated approach

9. Method:

9.1. Production target optimisation

9.1.1. Maximise muon and pion yield between 0 and 80 MeV at entrance to muon beamline

9.1.2. Parameters to vary: target length, target radius

9.2. Muon beam optimisation

9.2.1. Maximise muon stopping rate in stopping target

9.2.2. Minimise pion stopping rate

9.2.3. vary dipole along TS2 and TS4

9.2.4. vary Collimators: TS2 and at TS3

9.3. Electron spectrometer optimisation

9.3.1. Optimise dipole to increase signal acceptance

9.3.2. Optimse DIO blockers so DIO rate per straw is less than 1 kHz

9.3.3. Vary solenoidal field to increase separation?

9.4. Stopping target / beam blocker optimisation

9.4.1. Maximise reflection of signal electrons from upstream by tuning target position

9.5. Detector optimisation

2.2. Optimisation Goals

10. Set sensitivity goal and optimise to reach this

11. Single event sensitivity only considers signal acceptance, but also need to understand backgrounds in terms of final confidence limit that can be set

2.3. Production Target Optimisation

In the Phase-II Conceptual Design Report (CDR), the production target is given as being 16 cm in length and 4 mm in radius [**?**]. Since then, there have been changes to the magnetic field in this region, as well as the lengths and locations of solenoids, shielding and beam-pipe, and the proton beam. Previous studies have looked at comparing the Tungsten target proposed for Phase-II to other materials [**?**], and also drawn a comparison between MARS [**?**], Geant4 [**?**] and the limited data available.

The goal in this study then is to optimise the production target with the up-to-date configurations. This study aims to maximise the total muon and pion yield below 80 MeV at the entrance to the Torus1 bent solenoid, by varying the radius and length of the production target.

2.3.1. Configuration

Table 2.1 gives the key parameters for the beam input and other aspects of this simulation. The location and orientation of the target were held fixed, since the proton beamline is fixed with respect to the muon beam axis. Once a realistic proton beam becomes available, these values would also benefit from optimisation, however. During the scan over length, the back face of the target was kept 8 cm away from the muon beam since the radiation shielding has previously been optimised, and since beyond this the magnetic field will no longer be able to capture the pions and muons produced.

It must be noted that at this point in time there is a appreciable uncertainty in the proton beam profile and position. In particular, whilst the proton beamline upstream has

Proton Beam	
Horizontal spread, σ_x	5.8 mm
Vertical spread, σ_y	2.9 mm
Mean energy, μ_E	8.01 GeV
Energy spread, σ_E	0.135 MeV
Target	
Material	Tungsten
Orientation	10° between target's principal axis and the muon beam axis.
Location	Back face fixed 8 cm away from muon beam axis.
Length	16 cm in CDR. Varied in steps of 4 cm from 4 to 32 cm.
Radius	4 mm in CDR. Varied from 2 to 10 cm in steps of 2 cm and from 10 to 30 cm in steps of 4 cm.
Software configuration	
Packages	`heads/1512w51_develop(3a0ee59)__3_UNCOMMITTED__`
Externals	`heads/Patch_Geant4-G4MultiLevelLocator(11fc8f0)`
Fieldmap	160104 ***((CHECK:))***
Sample Sizes	
Length scan	3e5 Protons on Target (POT) (30 runs of 1e4)
Radius scan	4.9e5 POT (49 runs of 1e4)
Final scan	

Table 2.1.: Key parameters in the configuration of the Production Target optimisation.

been well delivered, the effect of the magnetic field and necessary dipole and quadrupole magnetics are still being studied by the proton beam-line group. The beam profile is given in the Phase-I Technical Design Report (TDR) as having a Gaussian profile and energy distribution, but no divergence or location is given. The effect of the proton beam distribution on the overall sensitivity shall therefore be considered later on.

Protons originated from a plane (distributed as a two dimensional Gaussian across this surface) but since there is therefore some scope to tune the proton beam's position, the input particle plane was moved to remain 1 cm away from the front surface of the target. Since the aim is to maximise the muon and pion yield by varying only the length and radius, shifting the proton beam input plane in this way removes any variation of target acceptance due to divergences of the proton beam in the magnetic field.

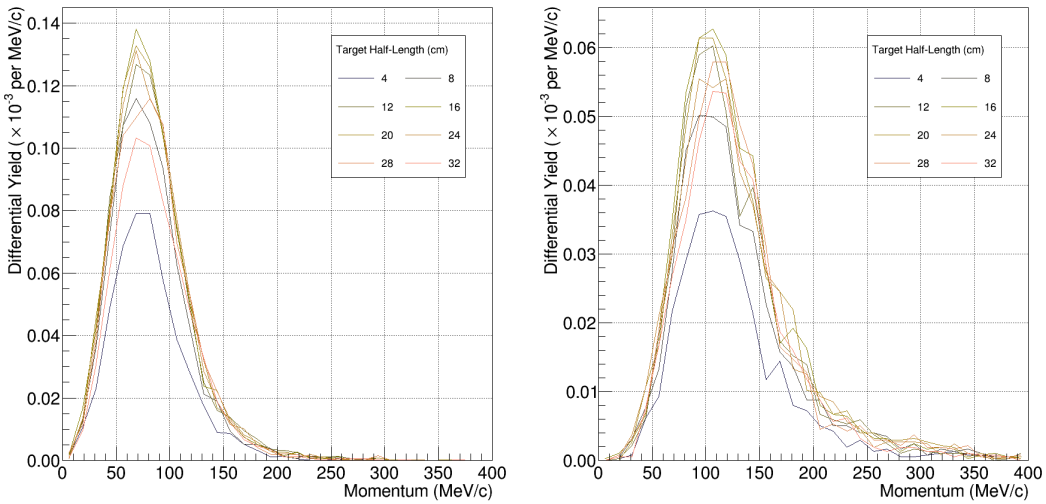

(a) Muons **(b)** Pions

Figure 2.1.: Change to momentum distributions at the entrance to the first 90 degrees of the bent muon beam solenoid for different target lengths. Target length is given as half-length which is the Geant4 convention.

2.3.2. Length Scan

Different length targets were simulated with 3e5 POT per length. Target length was varied in steps of 4 cm from 4 to 32 cm, whilst the target radius was held fixed at the CDR value of 4 mm.

Fig. **??** shows the momentum distributions of pions and muons for different target lengths. Target length is given as half-length which is the Geant4 convention. Fig. 2.2 then shows these distributions integrated up to different momentum. From these plots it can be seen that for both muons and pions, the optimum target length occurs around a total length of 32 cm.

Additionally it can be seen from Fig. 2.3 that the shape of the momentum distributions changes only weakly as a function of the target length. These plots were produced by normalising the integrated momentum contours of Fig. 2.2 to the total integral below 400 MeV. As a result, it is possible that the actual shape variation is even weaker than apparent here, since in the present sample size, the high momentum tail is not well sampled at small target lengths, such that a skew in the normalisation might occur.

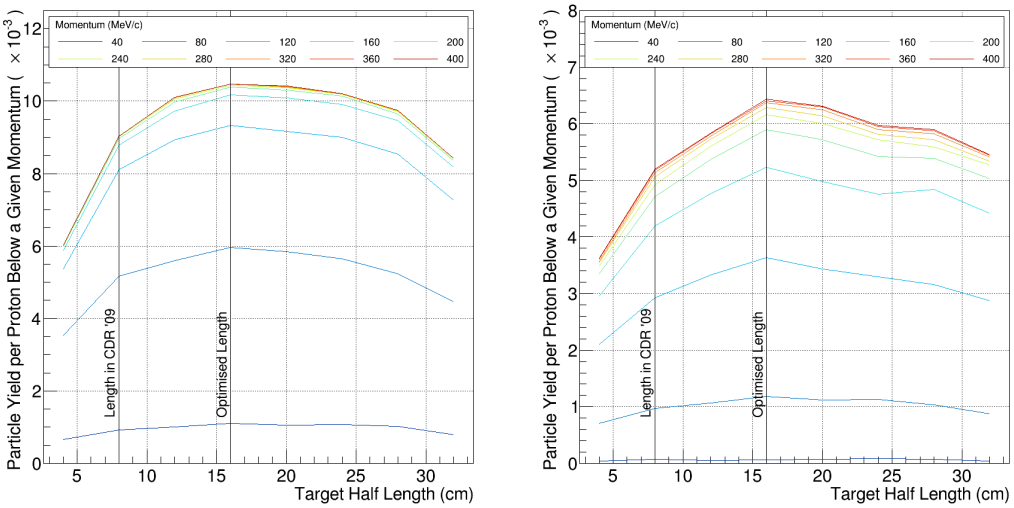

(a) Muons **(b)** Pions

Figure 2.2.: Integrated muon and pion yields up to a certain momentum at the entrance to the first 90 degrees of the bent muon beam solenoid as a function of target length.

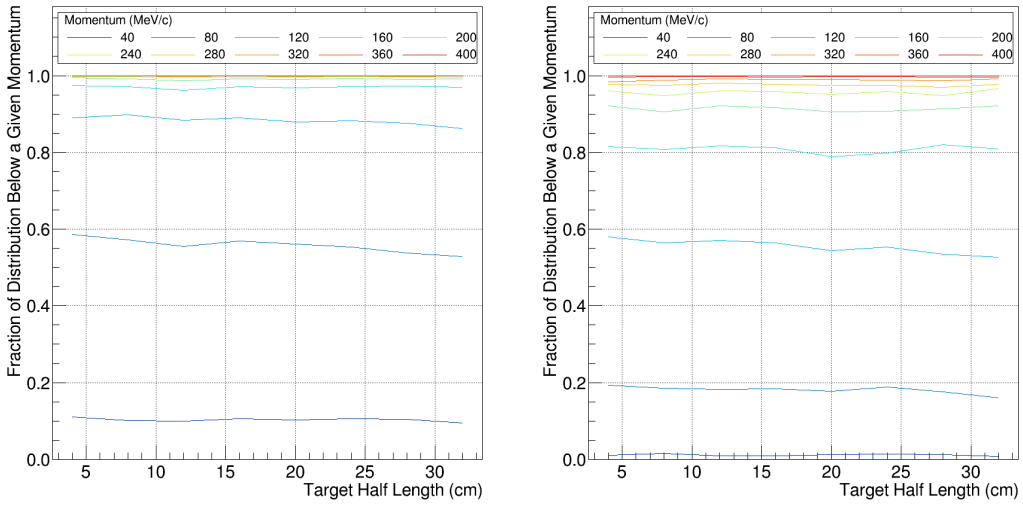

(a) Muons **(b)** Pions

Figure 2.3.: Change in the momentum distribution of muons and pions at the entrance to the first 90 degrees of the bent muon beam solenoid as a function of target length.

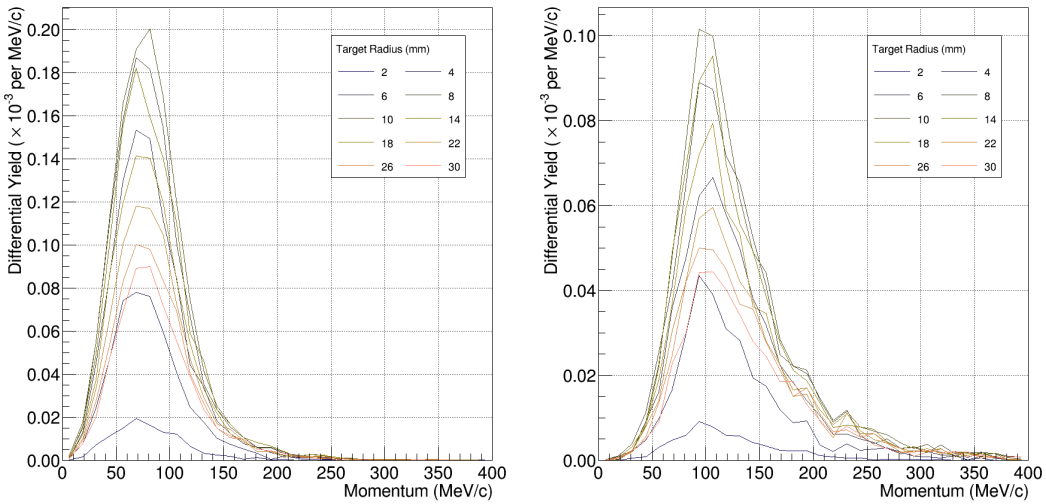

(a) Muons **(b)** Pions

Figure 2.4.: Change to momentum distributions at the entrance to the first 90 degrees of the bent muon beam solenoid for different target radii.

2.3.3. Radius scan

In parallel to the length optimisation scan, different radii targets were also simulated. Targets with radii of 2, 4, 6, 8, 10, 14, 18, 22, 26, and 30 mm were tested. The target length was held at the CDR value of 16 cm in total.

The results of these scans can be seen in Fig. **??** and Fig. 2.5, where it can be seen that a maximum in both the muon and pion yields at the entrance to the Torus1 section is achieved at a radius of about 10 mm. As in the length scan, the shape variation of the momentum distributions is rather weak as a function of target radius.

2.3.4. Final Result

Since the length and radius scan were performed in parallel, a final cross check was performed where the optimal radius was confirmed at the optimised target length. The integrated spectrum is shown in Fig. **??** where it can be seen that the optimum radius once the target length is increased to 32 cm is still 10 mm.

12. Figure comparing Phase-II to Phase-I

13. Conclusions

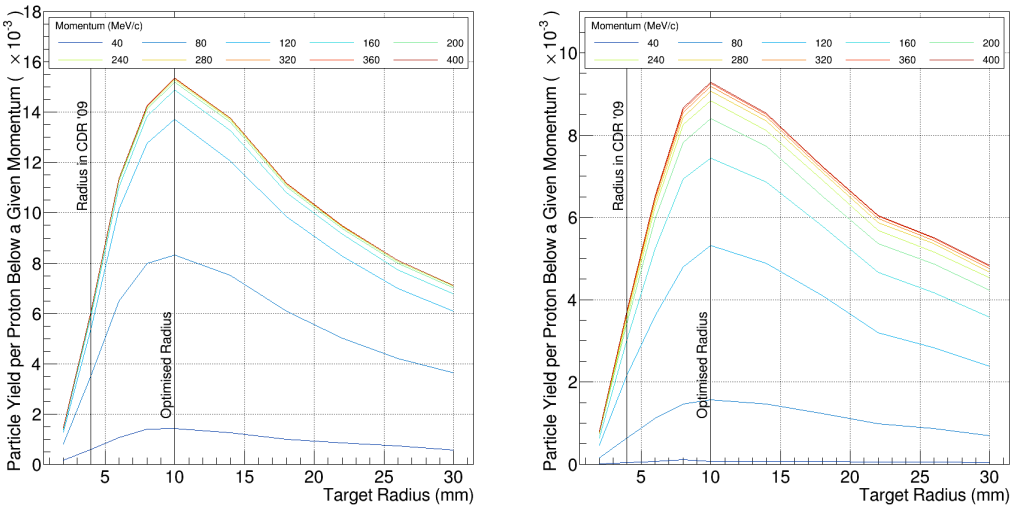

(a) Muons **(b)** Pions

Figure 2.5.: Integrated muon and pion yields up to a certain momentum at the entrance to the first 90 degrees of the bent muon beam solenoid as a function of target radius.

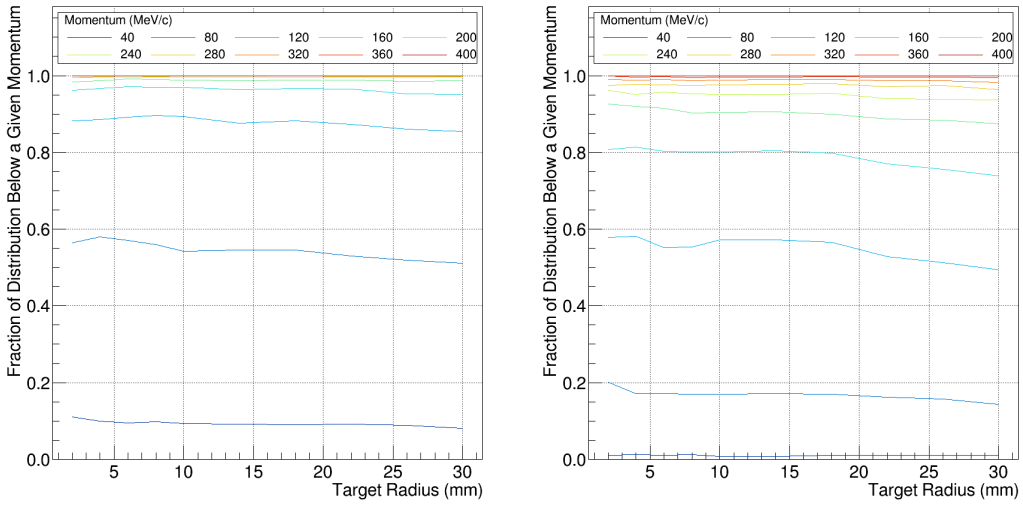

(a) Muons **(b)** Pions

Figure 2.6.: Change in the momentum distribution of muons and pions at the entrance to the first 90 degrees of the bent muon beam solenoid as a function of target radius.

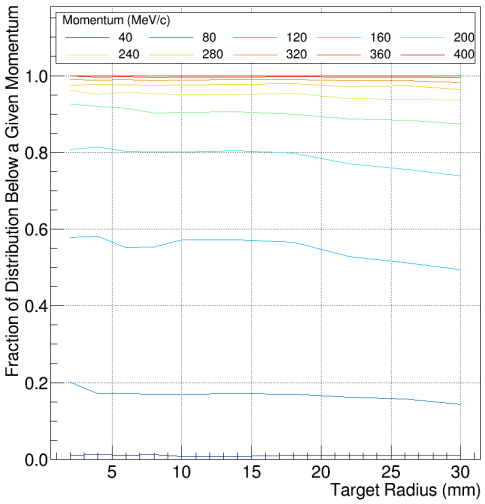

Figure 2.7.: Comparison of the combined muon and pion yield at the entrance to Torus1 for Phase-I (blue) and Phase-II (red).

Appendix A.

Drifts in a Bent Solenoid

The Lorentz force:

$$\frac{d\vec{p}}{dt} = \frac{q}{m}\vec{p} \times \vec{B} \tag{A.1}$$

A.1. Uniform Solenoidal Field

B field is uniform and parallel to axis of solenoid. Define the Larmor frequency, ω, and radius, a, as:

$$a = \frac{\gamma m \vec{v} \times \vec{B}}{qB^2} = \frac{p_{\mathrm{T}}}{qB} \tag{A.2}$$

$$\omega = \frac{qB}{m} \tag{A.3}$$

A.2. Field in a Bent Solenoid

Producing a cylindrical solenoid channel can be imagined as directly bending that of a normal uniform and linear one. By symmetry it can be seen that any gradient introduced to the magnetic field can only be radially, in the plane of the bending. Further, by considering Ampere's law with a current loop in the plane of bending formed by two radial straight lines (with length $|r - R| < L$, where R and L are the bending and aperture radii of the solenoid channel) and an arc, it can be seen that the variation in

the field is given by:

$$\frac{\vec{\nabla} B}{B} = \frac{1}{r}\hat{r} \tag{A.4}$$

((CHECK: Sketch or figure?))

A.3. Drift Calculation

There are two sources of drift in a bent solenoid: the gradient in the field, and the centrifugal force arising from the circular coordinate system needed to describe the field lines. The two can be treated separately in the sense that the motion of a particle moving through a field with straight field lines but with a transverse gradient given by $\nabla B/B \propto 1/r$ would be described by an equation of motion equivalent to that from the first source of drift in the bent solenoid system. Similarly, a system with a uniform field but field lines that follow circular paths would exhibit drift equivalent to the second component mentioned above.

A.3.1. Gradient Drift

"Grad-B" drift is well described in text books, but in the interest of completeness a short derivation shall be given here. The drift arising due to the gradient in the field can be treated as a perturbation of the motion of the particle in a uniform solenoidal field. The total velocity $\vec{V}$, is given by:

$$\vec{V} = \vec{v} + \vec{v_g}, \tag{A.5}$$

where $\vec{v}$ is the unperturbed velocity of the particle in the transverse plane, and $\vec{v_g}$ is the velocity arising due to the gradient in the field.

Treating the field as a Taylor expansion:

$$\vec{B}(\vec{r}) = \vec{B_0} + (\vec{r} \cdot \nabla)|_{\vec{r}=0}\, \vec{B} + \ldots \tag{A.6}$$

and substituting equations Eq. A.5 and Eq. A.6 into the Lorentz force, gives:

$$m\frac{d(\vec{v}+\vec{v_g})}{dt} = q(\vec{v}+\vec{v_g}) \times \left(\vec{B_0} + (\vec{r}\cdot\nabla)|_{\vec{r}=0}\,\vec{B}\right) \tag{A.7}$$

$$\tag{A.8}$$

so that to first order, the perturbing velocity is given by:

$$\frac{d\vec{v_g}}{dt} = \frac{q}{m}\left(\vec{v} \times (\vec{r}\cdot\nabla)|_{\vec{r}=0}\,\vec{B} + \vec{v_g} \times \vec{B_0}\right) \tag{A.9}$$

Since we are only interested in steady-state solutions where $dotv_g$ is close to zero, the above equation gives:

$$\vec{v_g} = \frac{q}{m}\frac{\vec{B_0} \times \left(\vec{v} \times (\vec{r}\cdot\nabla)|_{\vec{r}=0}\,\vec{B}\right)}{B_0^2} \tag{A.10}$$

which after time averaging becomes:

$$\langle\vec{v_g}\rangle_t = \frac{\vec{B_0} \times \left(\vec{v} \times (\vec{r}\cdot\nabla)|_{\vec{r}=0}\,\vec{B}\right)}{B_0^2} \tag{A.11}$$

List of Acronyms

CDR Conceptual Design Report

POT Protons on Target

TDR Technical Design Report

Bibliography

[1] Wilhelm H. Bertl et al. A Search for muon to electron conversion in muonic gold. *Eur.Phys.J.*, C47:337–346, 2006.